Break-Even Analysis of All-Solid-State Batteries with Li-Garnet Solid Electrolytes

ACS Energy LETTERS

http://pubs.acs.org/journal/aelccp

VIEWPOINT

Break-Even Analysis of All-Solid-State Batteries with Li-Garnet Solid Electrolytes

Cite This: *ACS Energy Lett.* 2021, 6, 2202−2207

Read Online

ACCESS | Metrics & More | Article Recommendations | Supporting Information

Presently, replacement of liquid electrolytes by their solid-state counterparts is pursued as a compelling way to improve energy densities, safety, and the cycle life of conventional Li-ion batteries (LIBs).[1] Toward this goal, rechargeable battery technologies based on solid-state electrolytes (SSEs), such as Li garnets,[2−8] LISICON ($Li_{14}ZnGe_4O_{16}$), thio-LISICON ($Li_{4-x}M_{1-x}P_xS_4$ (M = Ge, Si),[9,10] $Li_{10}GeP_2S_{12}$),[11] $Li_2S−P_2S_5$ glass,[12] $Li_7P_3S_{11}$ glass-ceramic,[13] argyrodites Li_6PS_5X (X = Cl, Br, I),[14,15] perovskites,[16,17] and antiperovskites,[18] have come into the research spotlight. In particular, batteries that employ the garnet-type $Li_7La_3Zr_2O_{12}$ (LLZO) SSE harness numerous advantages, such as high ionic conductivity of up to 1 mS cm^{-1} at room temperature (RT),[2,3,19−21] chemical stability with metallic lithium,[22,23] and low electronic conductivities of ca. 10^{-8} S cm^{-1} (RT).[24] Besides, LLZO has a wide electrochemical window (>6 V vs Li/Li^+ obtained in the experimental operation[25,26] and ∼3 V from computational analyses[27]), allowing for employment of high-voltage cathode materials, unlike other Li-ion solid-state conductors, such as those based on sulfides.[28,29]

Despite numerous studies on LLZO-based cells,[26,29−36] there is a lack of research on designing cells that possess practically relevant gravimetric and volumetric energy densities of >250 Wh kg^{-1} and 700 Wh L^{-1}, respectively. The vast majority of laboratory research in this area is conducted on millimeter-thick LLZO pellets, as they are readily produced by well-established high-temperature solid-state synthesis and are convenient for assembling symmetric and full cells for studying the performance of the SSE itself, as well its combinations with various electrode materials. Notwithstanding the rapidly improving performance of these cells, such thick pellets of SSEs (see Table S1) cannot be used in commercial solid-state batteries (SSBs) due to their high mass and hence the reduced and impractical overall energy density of the battery. Furthermore, tests with mm-thick pellets may lead to incorrect conclusions about the achievable performance of much thinner SSE membranes (20−50 μm), eventually required for commercial batteries, namely with regard to cycling stability and critical current density of the SSE. LLZO membranes are very brittle[37−40] and prone to the formation of cracks, which in turn results in the formation of Li-metal dendrites upon battery operation.[41−43] The other disparity with practical requirements stems from the common practice of using small areal capacities of cathodes in laboratory cells.[44−52] The typical performance of such thin electrodes (<1 mAh cm^{-2}) may not reach required areal capacities (>3.5 mAh cm^{-2}) at higher cathode mass loadings without proper engineering of interfaces and solid-state ionic transport.

In this Viewpoint, we comprehensively assess gravimetric and volumetric energy densities of Li-garnet SSBs, with the aim to aid further development and commercialization of this technology. In the analysis, we employ a battery configuration consisting of a metallic lithium anode, LLZO solid electrolyte, and LLZO composite cathode, as shown in Figure 1. The cathodic areal capacity and the thickness of the LLZO solid electrolyte are selected as two major variables of importance for the practical development of Li-garnet SSBs, for which the respective minimal and maximal values (break-even points) required to reach the energy density of conventional Li-ion batteries (ca. 250 and 700 Wh kg^{-1}) were determined. Another factor that hinders the commercial deployment of Li-garnet SSBs is finding a minimal yet sufficient LLZO content in the composite cathodes, and we outline these practical limits for $LiCoO_2$ (LCO), $LiNi_{0.33}Mn_{0.33}Co_{0.33}O_2$ (NMC111), $LiFePO_4$ (LFP), $LiNi_{0.5}Mn_{1.5}O_4$ (LMNO), FeF_3, and sulfur composite cathodes.

Figure 2 shows the energy density of an LLZO battery comprising a LCO cathode and Li anode vs the two key parameters identified as most relevant for maximizing the energy density: (i) the thickness of the LLZO dense layer separating the cathode and Li anode layers and (ii) the areal capacity of the cathode layer. The impact of varying the thickness of the Li metal anode is discussed later; for now, it is fixed that the Li anode areal capacity in the discharge state corresponds to 20% of the cathode's areal capacity. Hence, for cathodic areal capacities of 1, 3, and 5 mAh cm^{-2}, Li anode thickness equals 1, 3, and 5 μm, accordingly. In this configuration, ca. 83% of the total lithium amount (in both electrodes) should pass through the LLZO electrolyte upon the first charge of the battery. Aiming to assess the energy density of Li-garnet SSBs as realistically as possible, we considered the conventional composition of cathodes based on 95 wt% of cathode active material, 3 wt% of carbon black, and 2 wt% of the PVDF binder. Additional parameters that are not

Received: March 30, 2021
Accepted: April 9, 2021
Published: May 18, 2021

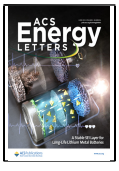

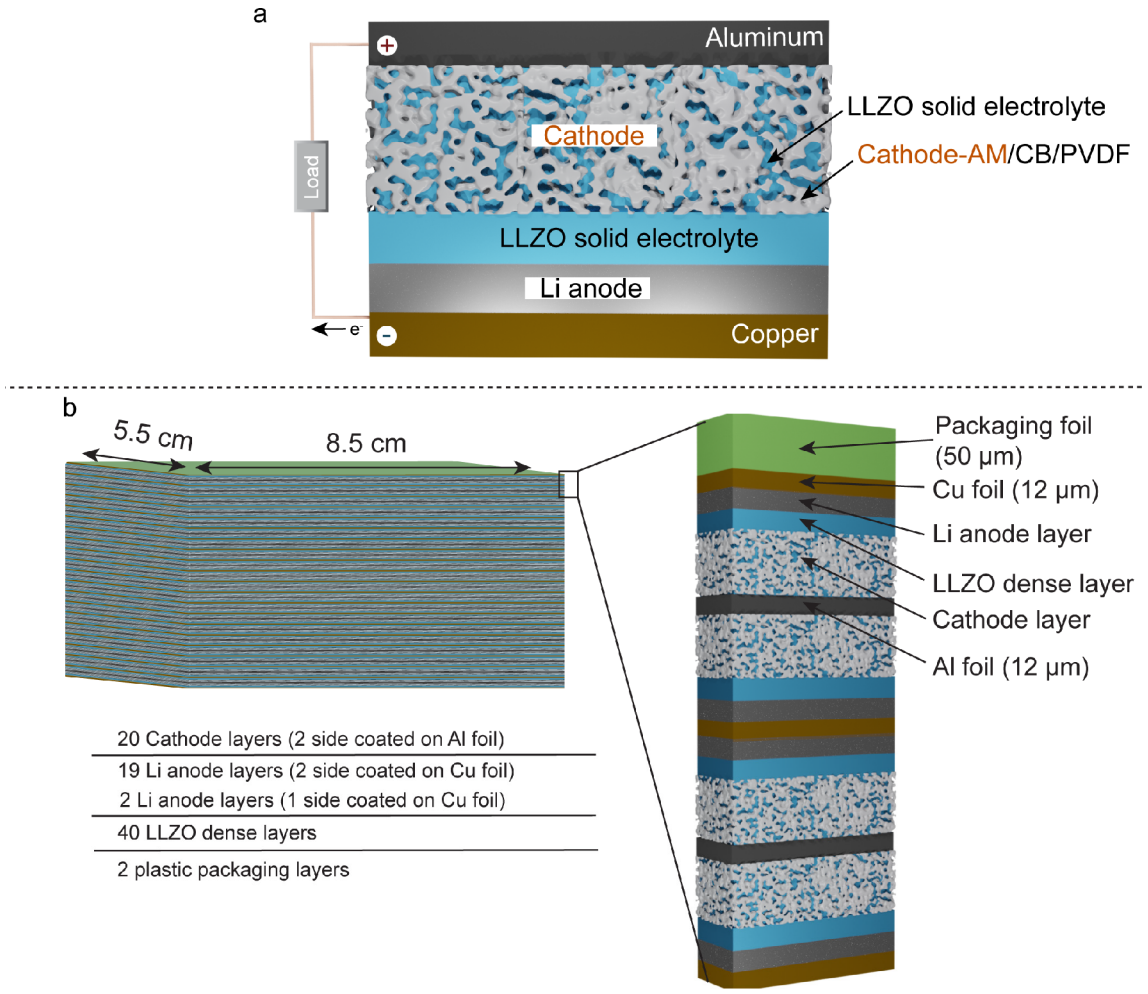

Figure 1. Schematics of the cell (a) and a battery (b) considered in this work for assessing the energy densities of Li-garnet SSBs. Cathode-AM is cathode active material. CB is carbon black. PVDF is polyvinylidene fluoride binder.

shown in Figure 2 include the thickness of Cu and Al foils and the thickness of pouch Al foil, and they were kept constant (see Table S2 for details).

The achievable gravimetric and volumetric energy densities were calculated from active material loading, active material utilization, assumed average cell voltage of 3.9 V, and total weight or volume of all cell components. The cell volume is calculated in the fully discharged state, which is the state in which the battery would be assembled. No kinetic or transport limitations are used in these calculations. Additionally, 100% of active material cathode utilization is assumed. A total of 40 cathode/electrolyte/anode layers was assumed (Figure 1). It should also be emphasized that employment of high areal capacities of >1 mAh cm^{-2} can be practically achieved only at pressures suitable to prevent the formation of voids/cavities at the LLZO/Li interface.[53−56] Utilization of pressure unavoidably results in added non-active components and hence decreases the energy density. Owing to the uncertainties as to the required and optimal pressures and thus the practical embodiment of this requirement, we omitted this parameter from the calculation of the energy density. Additionally, we note that, although the employment of the LLZO SSE allows for the design of high-voltage bipolar stacked batteries and thus further increasing their energy density,[57−59] the stacking of multiple cells within a single package has thus far been proven challenging.[60] Consequently, in this work, a conventional (monopolar) battery configuration that is employed in the current design of liquid LIBs is considered.

We first consider the LCO cathode with a porosity of 30%, assuming that the pores of the electrolyte are filled by three different electrolytes: 1 M $LiPF_6$ in ethylene carbonate/dimethyl carbonate (EC/DMC) conventional electrolyte, 0.3 M LiTFSI (lithium bis(trifluoromethanesulfonyl)imide) in PY14TFSI (*N*-butyl-*N*-methyl-pyrrolidiniumbis(trifluoromethanesulfonyl)imide) ionic liquid electrolyte, or LLZO SSE. In all cases, no unoccupied pore volume is assumed to exist. In Figure 2, the energy density of the battery is plotted vs cathode capacity and LLZO thickness. The LLZO thicknesses that allow the cell to attain the energy density of a conventional LIB (250 Wh kg^{-1} and 700 Wh L^{-1}) at a given cathode areal capacity are identified. Such a value is referred to as the break-even thickness, in analogy to the break-even point in economics, i.e., the point at which total cost and total revenue are equal.

The break-even thicknesses of the LLZO electrolyte for three different scenarios with respect to the gravimetric energy density are summarized in Figure 3a as a function of cathode areal capacity. As follows from Figure 3a, in the case of conventional liquid electrolyte in the cathode pores, the break-even LLZO thickness ranges from 31 to 51 μm for 3.5 mAh cm^{-2} and 5 mA cm^{-2}, accordingly. A similar break-even thickness range of 30−50 μm is obtained with ionic liquid

https://doi.org/10.1021/acsenergylett.1c00672
ACS Energy Lett. 2021, 6, 2202−2207

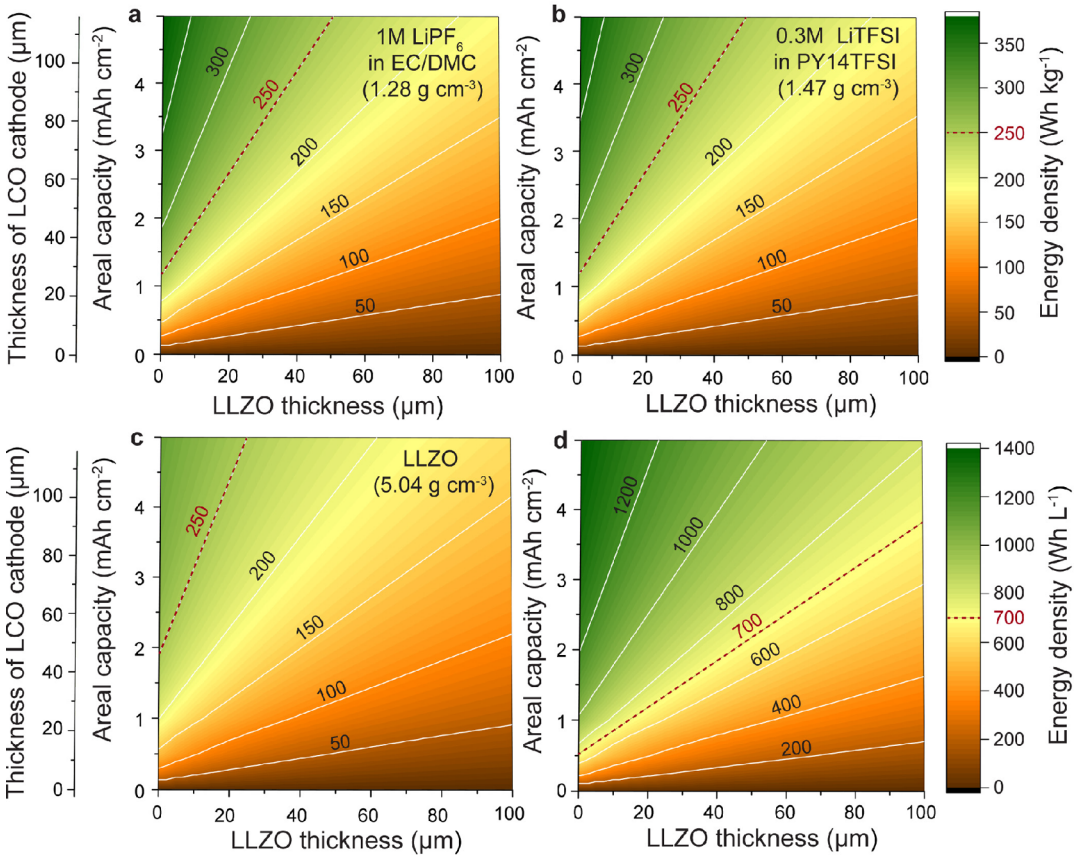

Figure 2. (a−c) Calculated gravimetric energy density of Li/LCO batteries vs cathode areal capacity and LLZO thickness. Batteries comprise 1 M $LiPF_6$ in EC/DMC (a), 0.3 M LiTFSI in PY14TFSI (b), and LLZO (c) electrolytes in the LCO cathode. (d) Volumetric energy density of Li/LCO batteries vs cathode areal capacity and LLZO thickness.

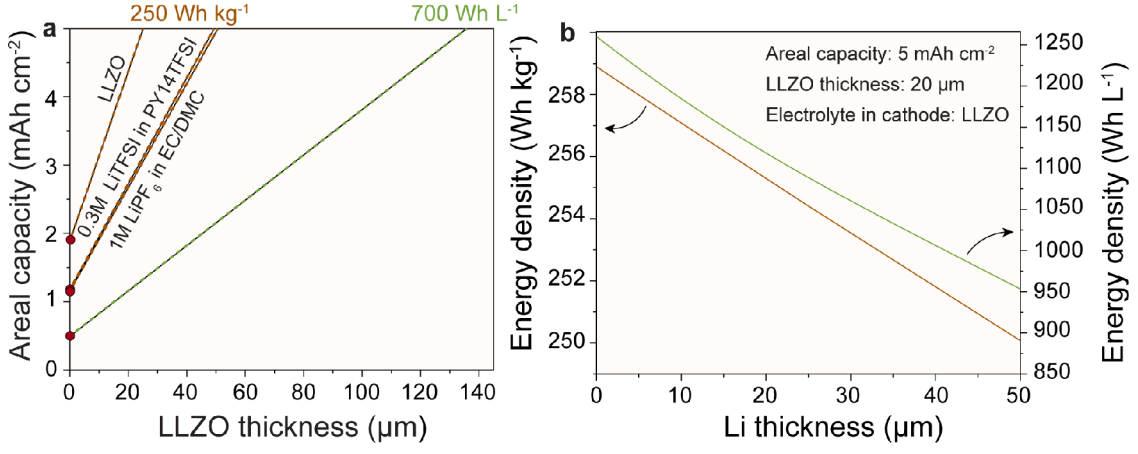

Figure 3. (a) Gravimetric and volumetric break-even thicknesses of LLZO electrolyte vs cathode area capacity for garnet-type Li metal batteries comprising LCO cathode impregnated with 1 M $LiPF_6$ in EC/DMC, 0.3 M LiTFSI in PY14TFSI, and LLZO electrolytes. (b) Change of gravimetric and volumetric energy densities of LCO-based Li-garnet SSBs vs Li anode thickness at fixed cathode areal capacity of 5 mAh cm^{-2} and LLZO thickness of 20 μm.

electrolyte as pore-filler. However, in the case of an all-solid-state system comprising LLZO electrolyte only, much lower thicknesses of 13−25 μm must be used in order to reach the same energy density of 250 Wh kg^{-1}. The volumetric energy density values are identical for batteries composed of either liquid or solid electrolytes, as the volume of batteries remains unchanged for all used electrolytes. Consequently, break-even LLZO thicknesses are identical for all three considered cases and equal 90−136 μm for 3.5 mAh cm^{-2} and 5 mA cm^{-2}, accordingly.

Interestingly, assuming that one can apply an infinitely thin LLZO layer, the break-even cathode areal capacity was found to be 1.16, 1.18, and 1.89 mAh cm^{-2} for the cells comprising carbonate-based, ionic liquid, and LLZO electrolytes in cathode pores. When comparing the same calculations for volumetric energy density, an areal capacity of 0.49 mAh cm^{-2} was found to be the break-even value. Of note, higher Li excess

https://doi.org/10.1021/acsenergylett.1c00672
ACS Energy Lett. 2021, 6, 2202−2207

has only a modest effect on gravimetric energy densities. For example, when the Li anode thickness was multiplied by 10, the gravimetric break-even LLZO thickness at a cathode areal capacity of 5 mAh cm^{-2} shifted from 24.6 to 20.0 μm, while the volumetric break-even thickness changed significantly from 135.7 to 92.1 μm (Figure S1). At the same time, at a fixed cathode areal capacity of 5 mAh cm^{-2} and LLZO thickness of 20 μm, the gravimetric energy density decreased from 258 Wh kg^{-1} to only 250 Wh kg^{-1} (Figure 3b). On the contrary, a significant reduction of the volumetric energy density (from 1220 to 953 Wh L^{-1}) was found for a 10-times thicker Li anode (50 μm instead of 5 μm).

Next, we analyzed the dependence of volumetric and gravimetric energy densities of solid-state LLZO cells on the porosity of the cathodes (LLZO electrolyte content) based on LCO, NMC111, LFP, LMNO, FeF_3, and S cathode active materials. Figures S2−S7 evidence that, upon an increase of LLZO content in a composite cathode, a higher areal capacity and a lower LLZO membrane thickness should be used to attain the same energy density values (250 Wh kg^{-1} and 700 Wh L^{-1}). Interestingly, assuming that the battery can be fabricated with a LLZO thickness as low as 10 μm and a high areal capacity of 5 mAh cm^{-2}, solid composite cathodes cannot have more than 40%, 46%, 40%, 56%, 79%, and 89% LLZO (by weight) to result in gravimetric energy densities that at least match those of conventional Li-ion batteries for LCO, NMC111, LFP, LMNO, FeF_3, and S cathodes, respectively. With regard to the volumetric energy density of 700 Wh kg^{-1}, the maximum permitted LLZO volume content lies at 66%, 68%, 45%, 71%, 83%, and 84% for LCO, NMC, LFP, LMNP, FeF_3, and S cathodes, respectively. It should be noted that the higher the thickness of LLZO, the lower should be the content of LLZO in the composite electrode. For example, Table S3 presents the recommended maximum LLZO content for various cathode active materials to achieve an energy density of 250 Wh kg^{-1} for 10- and 20-μm-thick LLZO layers. Importantly, the data on high-capacity conversion-type cathodes such as FeF_3 and S point to the fact that, hypothetically, up to 75−89% of LLZO weight content can be used in their electrodes. In the case of high-voltage intercalation-type LMNO cathodes, the maximum allowable LLZO volume content ranges from 53% to 56%. On the contrary, the LLZO content in conventional intercalation-type cathodes such as LCO, NMC, and LFP should not exceed 33−46%.

Summary and Outlook. While the literature on Li-garnet solid-state batteries has been flourishing in recent years, the development of their commercially competitive prototypes lags far behind. We reiterate that commonly reported tests on LLZO-based batteries as well as symmetrical cells employ mm-thick pellets and therefore do not provide practically relevant information on the achievable cycling stability and critical current density of μm-thin LLZO solid-state electrolytes required in commercially viable solid-state battery architectures. In this context, we encourage researchers working on Li-garnet solid-state batteries to focus investigations on LLZO membranes with a small thickness of 20−50 μm, which will allow discerning the entirety of truly relevant technical challenges at early stages, be it the membrane itself (synthesis, properties, interface engineering) or a suitable battery design and manufacturing process.

We further note that the employment of cathodes with a high areal capacity of >3.5 mAh cm^{-2} is imperative for reaching high gravimetric and volumetric energy densities of 250 Wh kg^{-1} and 700 Wh L^{-1}. Thus far, the laboratory LLZO-based cells utilized electrodes that have a very low areal capacity (on average 0.5−1 mAh cm^{-2}). As with the LLZO thickness, we recommend using thicker electrodes for early identification of the most relevant factors hampering the achievable energy and power densities and to outline cathode-material-specific research efforts.

We showed the maximal content of LLZO within the pores of a composite cathode that still permits matching the energy densities of the state-of-the-art Li-ion batteries (250 Wh kg^{-1}), as discussed for LCO, NMC111, LFP, LMNO, FeF_3, and sulfur composite cathodes. We also emphasize that minimization of the Li metal anode thickness in the Li-garnet batteries is not critical for their gravimetric energy density. The employment of thick commercial Li/Cu foils with a Li thickness of ca. 50 μm appears to be a practically viable approach. For instance, upon increasing the Li thickness from 5 to 50 μm, the gravimetric energy density decreases only slightly, from 259 to 250 Wh kg^{-1} (at a fixed cathode areal capacity of 5 mAh cm^{-2} and LLZO thickness of 20 μm). At the same time, the volumetric energy density is significantly reduced by ca. 306 Wh L^{-1} (from 1220 to 953 Wh L^{-1}).

Kostiantyn V. Kravchyk orcid.org/0000-0001-6149-193X
Faruk Okur
Maksym V. Kovalenko orcid.org/0000-0002-6396-8938

■ ASSOCIATED CONTENT

Supporting Information

The Supporting Information is available free of charge at https://pubs.acs.org/doi/10.1021/acsenergylett.1c00672.

Table S1, comparison of reported Li-garnet solid-state battery compositions; Table S2, parameters used in the energy density calculations; Table S3, recommended maximal LLZO content in cathodes; Figures S1−S7, calculated gravimetric and volumetric energy densities of batteries (PDF)

■ AUTHOR INFORMATION

Complete contact information is available at: https://pubs.acs.org/10.1021/acsenergylett.1c00672

Notes

Views expressed in this Viewpoint are those of the authors and not necessarily the views of the ACS.
The authors declare no competing financial interest.

■ ACKNOWLEDGMENTS

This research is part of the activities of the joint Empa-Fraunhofer ICS project "IE4B", which is financially supported under the ICON funding scheme.

■ REFERENCES

(1) Albertus, P.; Anandan, V.; Ban, C.; Balsara, N.; Belharouak, I.; Buettner-Garrett, J.; Chen, Z.; Daniel, C.; Doeff, M.; Dudney, N. J. Challenges for and pathways toward Li-metal-based all-solid-state batteries. *ACS Energy Lett.* **2021**, 1399−1404.
(2) Thangadurai, V.; Narayanan, S.; Pinzaru, D. Garnet-type solid-state fast Li ion conductors for Li batteries: critical review. *Chem. Soc. Rev.* **2014**, *43* (13), 4714−4727.

(3) Murugan, R.; Thangadurai, V.; Weppner, W. Fast lithium ion conduction in garnet-type $Li_7La_3Zr_2O_{12}$. *Angew. Chem., Int. Ed.* **2007**, *46* (41), 7778−7781.
(4) Ohta, S.; Kobayashi, T.; Asaoka, T. High lithium ionic conductivity in the garnet-type oxide $Li_{7-X}La_3(Zr_{2-X}, Nb_X)O_{12}$ (X = 0−2). *J. Power Sources* **2011**, *196* (6), 3342−3345.
(5) Allen, J. L.; Wolfenstine, J.; Rangasamy, E.; Sakamoto, J. Effect of substitution (Ta, Al, Ga) on the conductivity of $Li_7La_3Zr_2O_{12}$. *J. Power Sources* **2012**, *206*, 315−319.
(6) Ohta, S.; Kihira, Y.; Asaoka, T. Spontaneous formation of a core−shell structure by a lithium ion conductive garnet-type oxide electrolyte for co-sintering with the cathode. *J. Mater. Chem. A* **2021**, *9*, 3353−3359.
(7) Buschmann, H.; Berendts, S.; Mogwitz, B.; Janek, J. Lithium metal electrode kinetics and ionic conductivity of the solid lithium ion conductors "$Li_7La_3Zr_2O_{12}$" and $Li_{7-x}La_3Zr_{2-x}Ta_xO_{12}$ with garnet-type structure. *J. Power Sources* **2012**, *206*, 236−244.
(8) Buschmann, H.; Dölle, J.; Berendts, S.; Kuhn, A.; Bottke, P.; Wilkening, M.; Heitjans, P.; Senyshyn, A.; Ehrenberg, H.; Lotnyk, A.; et al. Structure and dynamics of the fast lithium ion conductor "$Li_7La_3Zr_2O_{12}$. *Phys. Chem. Chem. Phys.* **2011**, *13* (43), 19378−19392.
(9) Kanno, R.; Murayama, M. Lithium ionic conductor thio-LISICON: The Li_2S-GeS_2-P_2S_5 system. *J. Electrochem. Soc.* **2001**, *148* (7), A742.
(10) Murayama, M.; Sonoyama, N.; Yamada, A.; Kanno, R. Material design of new lithium ionic conductor, thio-LISICON, in the Li_2S−P_2S_5 system. *Solid State Ionics* **2004**, *170* (3), 173−180.
(11) Kamaya, N.; Homma, K.; Yamakawa, Y.; Hirayama, M.; Kanno, R.; Yonemura, M.; Kamiyama, T.; Kato, Y.; Hama, S.; Kawamoto, K.; Mitsui, A. A lithium superionic conductor. *Nat. Mater.* **2011**, *10* (9), 682−686.
(12) Hayashi, A.; Hama, S.; Morimoto, H.; Tatsumisago, M.; Minami, T. Preparation of Li_2S−P_2S_5 amorphous solid electrolytes by mechanical milling. *J. Am. Ceram. Soc.* **2001**, *84* (2), 477−79.
(13) Seino, Y.; Ota, T.; Takada, K.; Hayashi, A.; Tatsumisago, M. A sulphide lithium super ion conductor is superior to liquid ion conductors for use in rechargeable batteries. *Energy Environ. Sci.* **2014**, *7* (2), 627−631.
(14) Deiseroth, H.-J.; Kong, S.-T.; Eckert, H.; Vannahme, J.; Reiner, C.; Zaiß, T.; Schlosser, M. Li_6PS_5X: A class of crystalline Li-rich solids with an unusually high Li+ mobility. *Angew. Chem., Int. Ed.* **2008**, *47* (4), 755−758.
(15) Rao, R. P.; Adams, S. Studies of lithium argyrodite solid electrolytes for all-solid-state batteries. *Phys. Status Solidi A* **2011**, *208* (8), 1804−1807.
(16) Belous, A. G. Synthesis and electrophysical properties of novel lithium ion conducting oxides. *Solid State Ionics* **1996**, *90* (1), 193−196.
(17) Stramare, S.; Thangadurai, V.; Weppner, W. Lithium lanthanum titanates: a review. *Chem. Mater.* **2003**, *15* (21), 3974−3990.
(18) Zhao, Y.; Daemen, L. L. Superionic conductivity in lithium-rich anti-perovskites. *J. Am. Chem. Soc.* **2012**, *134* (36), 15042−15047.
(19) Taylor, N. J.; Stangeland-Molo, S.; Haslam, C. G.; Sharafi, A.; Thompson, T.; Wang, M.; Garcia-Mendez, R.; Sakamoto, J. Demonstration of high current densities and extended cycling in the garnet $Li_7La_3Zr_2O_{12}$ solid electrolyte. *J. Power Sources* **2018**, *396*, 314−318.
(20) Sharafi, A.; Haslam, C. G.; Kerns, R. D.; Wolfenstine, J.; Sakamoto, J. Controlling and correlating the effect of grain size with the mechanical and electrochemical properties of $Li_7La_3Zr_2O_{12}$ solid-state electrolyte. *J. Mater. Chem. A* **2017**, *5* (40), 21491−21504.
(21) Afyon, S.; Kravchyk, K. V.; Wang, S.; Broek, J. v. d.; Hänsel, C.; Kovalenko, M. V.; Rupp, J. L. M. Building better all-solid-state batteries with Li-garnet solid electrolytes and metalloid anodes. *J. Mater. Chem. A* **2019**, *7* (37), 21299−21308.
(22) Connell, J. G.; Fuchs, T.; Hartmann, H.; Krauskopf, T.; Zhu, Y.; Sann, J.; Garcia-Mendez, R.; Sakamoto, J.; Tepavcevic, S.; Janek, J. Kinetic versus thermodynamic stability of LLZO in contact with lithium Metal. *Chem. Mater.* **2020**, *32* (23), 10207−10215.
(23) Zhu, Y.; Connell, J. G.; Tepavcevic, S.; Zapol, P.; Garcia-Mendez, R.; Taylor, N. J.; Sakamoto, J.; Ingram, B. J.; Curtiss, L. A.; Freeland, J. W.; Fong, D. D.; Markovic, N. M.; et al. Dopant-dependent stability of garnet solid electrolyte interfaces with lithium metal. *Adv. Energy Mater.* **2019**, *9* (12), 1803440.
(24) Rangasamy, E.; Wolfenstine, J.; Sakamoto, J. The role of Al and Li concentration on the formation of cubic garnet solid electrolyte of nominal composition $Li_7La_3Zr_2O_{12}$. *Solid State Ionics* **2012**, *206*, 28−32.
(25) Thangadurai, V.; Pinzaru, D.; Narayanan, S.; Baral, A. K. Fast solid-state Li ion conducting garnet-type structure metal oxides for energy storage. *J. Phys. Chem. Lett.* **2015**, *6* (2), 292−299.
(26) Wang, C.; Fu, K.; Kammampata, S. P.; McOwen, D. W.; Samson, A. J.; Zhang, L.; Hitz, G. T.; Nolan, A. M.; Wachsman, E. D.; Mo, Y.; et al. Garnet-type solid-state electrolytes: materials, interfaces, and batteries. *Chem. Rev.* **2020**, *120* (10), 4257−4300.
(27) Zhu, Y.; He, X.; Mo, Y. Origin of outstanding stability in the lithium solid electrolyte materials: insights from thermodynamic analyses based on first-principles calculations. *ACS Appl. Mater. Interfaces* **2015**, *7* (42), 23685−23693.
(28) Xiao, Y.; Wang, Y.; Bo, S.-H.; Kim, J. C.; Miara, L. J.; Ceder, G. Understanding interface stability in solid-state batteries. *Nat. Rev. Mater.* **2020**, *5* (2), 105−126.
(29) Kim, K. J.; Balaish, M.; Wadaguchi, M.; Kong, L.; Rupp, J. L. M. Solid-state Li−metal batteries: Challenges and horizons of oxide and sulfide solid electrolytes and their interfaces. *Adv. Energy Mater.* **2021**, *11* (1), 2002689.
(30) Zhao, N.; Khokhar, W.; Bi, Z.; Shi, C.; Guo, X.; Fan, L.-Z.; Nan, C.-W. Solid garnet batteries. *Joule* **2019**, *3* (5), 1190−1199.
(31) Shen, X.; Zhang, Q.; Ning, T.; Liu, T.; Luo, Y.; He, X.; Luo, Z.; Lu, A. Critical challenges and progress of solid garnet electrolytes for all-solid-state batteries. *Mater. Today Chem.* **2020**, *18*, 100368.
(32) Duan, H.; Oluwatemitope, F.; Wu, S.; Zheng, H.; Zou, Y.; Li, G.; Wu, Y.; Liu, H. Li/Garnet interface optimization: An overview. *ACS Appl. Mater. Interfaces* **2020**, *12* (47), 52271−52284.
(33) Kim, A.; Woo, S.; Kang, M.; Park, H.; Kang, B. Research progresses of garnet-type solid electrolytes for developing all-solid-state Li batteries. *Front. Chem.* **2020**, *8*, 468.
(34) Samson, A. J.; Hofstetter, K.; Bag, S.; Thangadurai, V. A bird's-eye view of Li-stuffed garnet-type $Li_7La_3Zr_2O_{12}$ ceramic electrolytes for advanced all-solid-state Li batteries. *Energy Environ. Sci.* **2019**, *12* (10), 2957−2975.
(35) Liu, Q.; Geng, Z.; Han, C.; Fu, Y.; Li, S.; He, Y.-b.; Kang, F.; Li, B. Challenges and perspectives of garnet solid electrolytes for all solid-state lithium batteries. *J. Power Sources* **2018**, *389*, 120−134.
(36) Xu, L.; Li, J.; Deng, W.; Shuai, H.; Li, S.; Xu, Z.; Li, J.; Hou, H.; Peng, H.; Zou, G.; Ji, X. Garnet solid electrolyte for advanced all-solid-state Li batteries. *Adv. Energy Mater.* **2021**, *11* (2), 2000648.
(37) Fu, Z.; Zhang, L.; Gritton, J. E.; Godbey, G.; Hamann, T.; Gong, Y.; McOwen, D.; Wachsman, E. Probing the mechanical properties of a doped $Li_7La_3Zr_2O_{12}$ garnet thin electrolyte for solid-state batteries. *ACS Appl. Mater. Interfaces* **2020**, *12* (22), 24693−24700.
(38) Kerman, K.; Luntz, A.; Viswanathan, V.; Chiang, Y.-M.; Chen, Z. Review—practical challenges hindering the development of solid state Li ion batteries. *J. Electrochem. Soc.* **2017**, *164* (7), A1731−A1744.
(39) Yi, E.; Wang, W.; Kieffer, J.; Laine, R. M. Flame made nanoparticles permit processing of dense, flexible, Li^+ conducting ceramic electrolyte thin films of cubic-$Li_7La_3Zr_2O_{12}$ (c-LLZO). *J. Mater. Chem. A* **2016**, *4* (33), 12947−12954.
(40) Yi, E.; Wang, W.; Kieffer, J.; Laine, R. M. Key parameters governing the densification of cubic-$Li_7La_3Zr_2O_{12}$ Li^+ conductors. *J. Power Sources* **2017**, *352*, 156−164.
(41) Golozar, M.; Paolella, A.; Demers, H.; Savoie, S.; Girard, G.; Delaporte, N.; Gauvin, R.; Guerfi, A.; Lorrmann, H.; Zaghib, K.

https://doi.org/10.1021/acsenergylett.1c00672
ACS Energy Lett. 2021, 6, 2202−2207

Direct observation of lithium metal dendrites with ceramic solid electrolyte. *Sci. Rep.* **2020**, *10* (1), 18410.
(42) Cao, D.; Sun, X.; Li, Q.; Natan, A.; Xiang, P.; Zhu, H. Lithium dendrite in all-solid-state batteries: growth mechanisms, suppression strategies, and characterizations. *Matter* **2020**, *3* (1), 57−94.
(43) Krauskopf, T.; Dippel, R.; Hartmann, H.; Peppler, K.; Mogwitz, B.; Richter, F. H.; Zeier, W. G.; Janek, J. Lithium-metal growth kinetics on LLZO garnet-type solid electrolytes. *Joule* **2019**, *3* (8), 2030−2049.
(44) Kim, K. J.; Rupp, J. L. M. All ceramic cathode composite design and manufacturing towards low interfacial resistance for garnet-based solid-state lithium batteries. *Energy Environ. Sci.* **2020**, *13* (12), 4930−4945.
(45) Han, F.; Yue, J.; Chen, C.; Zhao, N.; Fan, X.; Ma, Z.; Gao, T.; Wang, F.; Guo, X.; Wang, C. Interphase engineering enabled all-ceramic lithium battery. *Joule* **2018**, *2* (3), 497−508.
(46) Liu, T.; Ren, Y.; Shen, Y.; Zhao, S.-X.; Lin, Y.; Nan, C.-W. Achieving high capacity in bulk-type solid-state lithium ion battery based on $Li_{6.75}La_3Zr_{1.75}Ta_{0.25}O_{12}$ electrolyte: Interfacial resistance. *J. Power Sources* **2016**, *324*, 349−357.
(47) Liu, T.; Zhang, Y.; Zhang, X.; Wang, L.; Zhao, S.-X.; Lin, Y.-H.; Shen, Y.; Luo, J.; Li, L.; Nan, C.-W. Enhanced electrochemical performance of bulk type oxide ceramic lithium batteries enabled by interface modification. *J. Mater. Chem. A* **2018**, *6* (11), 4649−4657.
(48) Ren, Y.; Liu, T.; Shen, Y.; Lin, Y.; Nan, C.-W. Garnet-type oxide electrolyte with novel porous-dense bilayer configuration for rechargeable all-solid-state lithium batteries. *Ionics* **2017**, *23* (9), 2521−2527.
(49) Kato, T.; Iwasaki, S.; Ishii, Y.; Motoyama, M.; West, W. C.; Yamamoto, Y.; Iriyama, Y. Preparation of thick-film electrode-solid electrolyte composites on $Li_7La_3Zr_2O_{12}$ and their electrochemical properties. *J. Power Sources* **2016**, *303*, 65−72.
(50) Ohta, S.; Komagata, S.; Seki, J.; Saeki, T.; Morishita, S.; Asaoka, T. All-solid-state lithium ion battery using garnet-type oxide and Li_3BO_3 solid electrolytes fabricated by screen-printing. *J. Power Sources* **2013**, *238*, 53−56.
(51) Liu, T.; Zhang, Y.; Chen, R.; Zhao, S.-X.; Lin, Y.; Nan, C.-W.; Shen, Y. Non-successive degradation in bulk-type all-solid-state lithium battery with rigid interfacial contact. *Electrochem. Commun.* **2017**, *79*, 1−4.
(52) Inada, R.; Yasuda, S.; Tojo, M.; Tsuritani, K.; Tojo, T.; Sakurai, Y. Development of lithium-stuffed garnet-type oxide solid electrolytes with high ionic conductivity for application to all-solid-state batteries. *Front. Energy Res.* **2016**, *4*, 28.
(53) Wang, M. J.; Choudhury, R.; Sakamoto, J. Characterizing the Li-solid-electrolyte interface dynamics as a function of stack pressure and current density. *Joule* **2019**, *3* (9), 2165−2178.
(54) Zhang, X.; Wang, Q. J.; Harrison, K. L.; Roberts, S. A.; Harris, S. J. Pressure-driven interface evolution in solid-state lithium metal batteries. *Cell Rep. Phys. Sci.* **2020**, *1* (2), 100012.
(55) Krauskopf, T.; Richter, F. H.; Zeier, W. G.; Janek, J. Physicochemical concepts of the lithium metal anode in solid-state batteries. *Chem. Rev.* **2020**, *120* (15), 7745−7794.
(56) Krauskopf, T.; Hartmann, H.; Zeier, W. G.; Janek, J. Toward a fundamental understanding of the lithium metal anode in solid-state batteries—an electrochemo-mechanical study on the garnet-type solid electrolyte $Li_{6.25}Al_{0.25}La_3Zr_2O_{12}$. *ACS Appl. Mater. Interfaces* **2019**, *11* (15), 14463−14477.
(57) Zhang, Z.; Shao, Y.; Lotsch, B.; Hu, Y.-S.; Li, H.; Janek, J.; Nazar, L. F.; Nan, C.-W.; Maier, J.; Armand, M.; Chen, L. New horizons for inorganic solid state ion conductors. *Energy Environ. Sci.* **2018**, *11* (8), 1945−1976.
(58) Famprikis, T.; Canepa, P.; Dawson, J. A.; Islam, M. S.; Masquelier, C. Fundamentals of inorganic solid-state electrolytes for batteries. *Nat. Mater.* **2019**, *18* (12), 1278−1291.
(59) Schnell, J.; Günther, T.; Knoche, T.; Vieider, C.; Köhler, L.; Just, A.; Keller, M.; Passerini, S.; Reinhart, G. All-solid-state lithium-ion and lithium metal batteries − paving the way to large-scale production. *J. Power Sources* **2018**, *382*, 160−175.
(60) Jung, K.-N.; Shin, H.-S.; Park, M.-S.; Lee, J.-W. Solid-state lithium batteries: Bipolar design, fabrication, and electrochemistry. *ChemElectroChem* **2019**, *6* (15), 3842−3859.

https://doi.org/10.1021/acsenergylett.1c00672
ACS Energy Lett. 2021, 6, 2202−2207